Original article

EVALUATION OF SELF-HEALING CORROSION PROTECTION USING BENZOTRIAZOLE-LOADED MESOPOROUS SILICA NANOCONTAINERS FOR APPLICATION ON ARCHAEOLOGICAL BRONZE ARTEFACTS

Rifai, M.

Conservation dept., Faculty of Archaeology, Cairo Univ., Giza, Egypt
E-mail address: mai.rifai@cu.edu.eg

EJARS – Vol. 14 (2) – Dec. 2024: 199-206

Abstract:

This work evaluates the effectiveness of coating bronze coupons, with 3% Benzotriazole (BTA)-loaded nanocontainers mixed with Paraloid polymer. Mesoporous silica nanoparticles (MSNs) were prepared and loaded with 3% BTA (BTA @MSNs) followed by dispersion in 3% Paraloid B72 and B44. Bronze disc samples with the chemical composition of Cu 85%, Sn 10% and Pb 5% simulating archaeological artifacts were coated with a single and double layer of BTA @MSNs in Paraloid B72 and B44 and evaluated using several techniques. Colorimetric measurements (CM) were used to evaluate changes in the surface appearance following the coating with single and double protective layers. The corrosion inhibitive performance of the coating was investigated using electrochemical impedance spectroscopy (EIS). Transmission electron microscope (TEM) was performed to characterize the shape and size of the prepared SiO_2 nanoparticles, while X-ray Diffraction (XRD) was performed to confirm the presence of amorphous mesoporous SiO_2 nanoparticles. The specific surface area, pore volume and pore size distribution were measured by nitrogen adsorption– desorption technique, while the release rate of benzotriazole at various experimental pH values was estimated using UV–Vis spectroscopy. Results confirmed the sustained release of benzotriazole to varying pH levels. The release was higher with an increase in the pH of the medium, which signifies that the release rate rises in the alkaline medium. The best corrosion inhibitive performance was for the double layer BTA @MSNs – B72 samples at 91.73% efficiency, while single layer BTA @MSNs – B72 samples displayed the least change in color ΔE 3.28.

1. Introduction

Standard anticorrosion coatings passively prevent the interaction of corrosive species with the metal [1], but do not offer sufficient protection over long periods of time due to aging, the formation of micro-pores and cracks, and areas of low cross-linking density, which provide a path for diffusion of corrosive species such as water, oxygen, and chloride ions to the coating/metal interface [2]. Corrosion processes, in particular, develop fast after disruption of the protective barrier [3]. Moreover, the direct addition of corrosion inhibitors to coatings often leads to coating degradation, inhibitor deactivation, or undesired leaching [4,5]. Direct introduction of the inhibitor into the coating matrix shows successful results for some classes of inhibitors; however, there are difficulties with the application of inhibitors with very high or low solubility in coatings [6,7]. A very low solubility of the inhibitor leads to its deficit in the damaged area. In cases of too high solubility, metal substrates can be protected for only a relatively short time due to the rapid spontaneous

leaching of inhibitor from the coating [8]. Another drawback, which can appear due to high solubility, is the osmotic pressure initiating blistering and, finally, delamination of the coating [9,10]. Recent studies investigated avoiding the direct interaction of the polymer and inhibitor by the encapsulation of the inhibitors within inert host nanostructures, generally referred to as nanocontainers, to control the release of the active component, i.e., the inhibitor activated by an external corrosion-related stimulus. There are numerous reports validating the favorable effect of inhibitor encapsulation on the quality of coatings in comparison to cases in which an inhibitor is added directly to the coating [11]. The immediate advantage of nanocontainers is the possibility of controlling the release of the active material. Once corrosion reactions commence, such nanostructures allow a controllable leaching of the inhibitor triggered by corrosion related stimuli [12,13]. Triggers could be in the form of mechanical damage of the coating, fluctuations in relative humidity, temperature or change in pH [15].

Among all of the stimulus response coatings, the pH-responsive coatings are the most significant, since the corrosion reaction on the metal surface usually causes the changes of the pH value in the cathodic and anodic areas [15]. In corrosion cases, dissolved oxygen or H+ ions are involved in the corrosion reaction. The cathodic reaction results in an increase in pH at the metal surface, while the oxidation of the metal at the anodic site often leads to a decrease in pH [16]. Therefore, the development of nanostructures that incorporate pH-responsive complexes facilitates the release of corrosion inhibitors at the active corrosion sites, allowing pH-sensitive systems to activate a self-healing mechanism as soon as the corrosion process begins [17]. Researchers developed complex systems, by adjusting the response of the nanocontainers with respect to specific conditions, aiming to release the corrosion inhibitors in conditions similar to specific corrosion mechanisms. As a result, various studies were focused on optimizing the release of corrosion inhibitors in acidic, alkaline or both environments [18]. Corrosion inhibitors are usually encapsulated within polymeric microcapsules [19] or inorganic meso- and nanoporous materials [20], such as mesoporous silica and TiO$_2$ nanotubes. Mesoporous silica nanocontainers (MSNs), which can be synthetized by a modified Stober process [21], by hydrolysis and condensation of silica precursors [22], gained widespread interest because of their large surface area, high pore volume, low density and stability favorable for the storage of healing agents [23]. Their well-controlled pore size, narrow pore size distribution, controllable functionality, and pore surface chemistries promote their use as the encapsulating material for controlled release of corrosion inhibitors. These encapsulated corrosion inhibitors can be added to different coating materials to promote long-term protection [24,25]. MSN can be synthetized by a modified Stober process [21], by hydrolysis and condensation of silica precursors [22]. Usually tetraethylorthosilicate (TEOS) or tetramethylorthosilicate (TMOS) [26] are used, but also other precursors are often reported. Moreover, surfactant, micelles forming materials, polymers or other dopants [27] are added to the selected precursors. In particular, the most used surfactant is cetyltrimethylammonium bromide (CTAB) [28]. In the mesoporous silica nanoparticles growth, by selecting adequately the pH, the condensation of silicon is enhanced with respect to the Stober process, promoting the formation of Si–O–Si bonds, instead of Si–OH [29]. The pores are then formed with the template removal in the nanoparticle structure through calcination or by solvent extraction [26]. In all cases, micro- and nanocontainers are first filled with an active agent and then dispersed in the whole coating matrix. The capsules are filled in different ways, e.g., by agitating the suspension of capsules and fillers, also under reduced pressure, the soaking of capsules in inhibitor solution, and by applying the LBL deposition procedure [30,17]. The evaluation of the corrosion protection efficiency of the anticorrosive systems is usually performed on metallic substrates according to specific field applications [26] using various analytical techniques, including electrochemical, morphological and spectroscopic. The morphological and structural properties of the prepared nanocontainers are characterized by various techniques such as scanning electron microscope (SEM), transmission electron microscope (TEM), X-ray diffraction (XRD) and nitrogen adsorption-desorption and Fourier transform infrared spectroscopy (FTIR) [31], while the evaluation of inhibitor release as a function of pH is examined via ultraviolet- visible (UV-vis) spectroscopy [31]. When dealing with cultural heritages, however, further restrictive characteristics of the protective layer are needed. Specifically, besides the corrosion protection, the coating has to be optically transparent in order to preserve the appearance of the artifact, and it has to be easily removable without compromising the integrity of the metallic surface [32]. The main objective of the present work is to establish the applicability of using intelligent release systems for the long-term protection of bronze archaeological artifacts against corrosion by preventing the uncontrolled leaching of inhibitor from the coating material.

2. Materials and Methods
2.1. *Materials*
Bronze alloy coupons were cast based on the chemical composition of archaeological bronze artefacts into 20mm diameter circular rods, then cut into disc-shaped samples of 2mm thickness. The cast samples were subjected to elemental analysis using Energy Dispersive X-ray to verify the composition after casting. The coupons were polished using emery paper of different grades up to 1200, then washed with alcohol in an ultrasonic bath, degreased with acetone and kept in a desiccator to prevent atmospheric corrosion. Tetraethylorthosilicate (TEOS) was used as a silica precursor. N, Cetyltrimethylammonium bromide (CTAB) a surfactant used in nanoparticles synthesis (pore generating agent) with sodium hydroxide (NaOH). Benzotriazole (BTA) 'Sigma-Aldrich' a heterocyclic compound, $C_6H_5N_3$, is an effective corrosion inhibitor for copper and its alloys, the solvent used was ethyl alcohol. Paraloid™ B-72 'Dow', and Paraloid™ B-44 'Dow', in ethyl alcohol. All chemicals that were used in this work are analytical grade reagents.

2.2. *Synthesis of mesoporous silica nanoparticles (MSNs)*
Synthesis of mesoporous silica nanoparticle was prepared from reaction mixture with optimum concentrations of reagents as outlined in tab. (1) CTAB was dissolved in water. Aqueous NaOH (2.0 M) was added to the CTAB solution, and the solution temperature was adjusted to 80°C in a silicon oil bath with stirring using a magnetic stirrer at 800 rotations per minute (rpm). The solution was heated for 30 min after which TEOS was added dropwise, and the mixture was allowed to stir for 2 h at 80°C. The resultant white precipitate was isolated by vacuum filtration using a Buckner funnel and washed several times with copious amount of water. The product was dried in an oven for 2 h at 140°C and ground into powder using a pestle and a mortar. Calcination of the material was performed at 550°C for 5 h to remove the template [33].

Sample code	CTAB mM	TEOS mM	NaOH mM	H2O moles
MPS	2.74	27.09	3.8	21.11

2.3. Synthesis of BTA-loaded MSNs (BTA@MSNs)
The processes for loading BTA into MSNs were as follows: 0.9 g of MSNs was dispersed in 100 mL of deionized water and 10 mL of methanol. 100 mg of BTA was then dissolved in the mixture. The mixture was adjusted to pH 7.5 and then stirred for 12 h. The mixture was centrifuged, washed by deionized water and vacuum-dried at 40 °C to obtain BTA-loaded MSN (BTA@MSNs).

2.4. Preparation of self-healing coatings and coating of bronze coupons
The assembled BTA@MSNs was dispersed into 3% Paraloid B72 and B44 in acetone by sonication. The final material was applied onto the cast disc-shaped bronze coupons wt.% Cu 85, Sn 10, and Pb 5. in a single and double layer by brushing with a 72 h interval between layers. The samples were left to completely cure for a week (ASTM D1640-95). [34]

2.5. Characterization
The surface morphology (size and shape) of the mesoporous nanoparticles was examined using a TEM JEOL JEM-2100 high resolution transmission electron microscope at an accelerating voltage of 200 kV, respectively. X-ray diffraction was performed using XPERT-PRO Powder Diffractometer system, with 2 theta ($20°-80°$), minimum step size 2Theta: 0.001, and at wavelength ($K\alpha$)= $1.54614°$. The specific surface area, pore volume and pore size distribution were measured by nitrogen adsorption– desorption technique. The samples were degassed at 453 K for 6 h under vacuum before analysis, the N2 isotherms were obtained at –196 °C. The specific surface area was calculated using the BET (Brunauer–Emmett–Teller) method. The pore size distributions were determined by applying the BJH (Barrett–Joyner–Halenda) model to the nitrogen desorption branch. To determine the amount of BTA encapsulated in the MSN a UV-vis spectrophotometer (Cary series UV-Vis- NIR, Australia) was used. A calibration curve was prepared for BTA ranging from a concentration of 1 µg mL^{-1} to 50 µg mL^{-1} (in 3.5% NaCl aqueous solution). After the separation of NPs from the reaction mixture, the absorbance of the supernatant was recorded at 259 nm and the concentration of free BTA was estimated based on the standard curve. Then EE and LC were calculated according the equation (1) [35].

$$\text{Entrapment efficiency} = \frac{\textit{intial Conc.} - \textit{free concentration}}{\textit{Intial Conc}} * 100 \ (1)$$

Loading capacity (LC%). The amount of total entrapped inhibitor was divided by the total nanoparticle weight.

2.6. Release Study
To examine the amount of BTA released by external pH variation, 1.0 g of BTA@ MSN was dispersed into 15 mL 3.5 wt% NaCl solution with different pH values (pH 5.0, 7.0 and 9.0 respectively) adjusted by HCl or NaOH solution. The suspension was placed into a dialysis bag (MWCO 10: 12 KDa) which was directly immersed into 60 mL of the corresponding solution at 25 °C. The UV–vis absorbance of the released BTA solution was recorded at 259 nm to determine the concentration of BTA at time t (Ci). The cum-ulative release percentage of BTA is calculated according to the equation (2).

$$\textit{Cumulative release} = \frac{V0C0. + V \ Sum \ (Ci - 0)}{m} * 100 \ (2)$$

Where m is the initial loading amount of BTA in the nanocontainers (g), Vo represents the total volume of the release solution (Vo = 75.0 mL) and V is the volume per sampling (V = 1.0 mL).

Colorimetric measurements
Color measurements were used to monitor the behavior or possible change in color instigated by the application of protective coatings. A CS-10 Digital Handheld (CHN Spec) Color Difference Meter SCI Lab, Aperture 8mm. was used. It measures the sample color data L*a*b*, color difference ΔE and ΔLab according to CIE color space. For each coupon, three measurements were conducted at different spots and the mean value was calculated. To characterize the color variation before and after treatment, the parameter ΔE* (color difference) was determined using the CIE equation (3).

$$\Delta E^* = \sqrt{(\Delta L^*)^2 + (\Delta a^*)^2 + (\Delta b^*)^2} \ (3)$$

2.7. Electrochemical Impedance Spectroscopy
Electrochemical Impedance Spectroscopy (EIS) was used to evaluate the efficiency of the nano capsule-impregnated coatings for the protection of bronze against corrosion. (EIS) measurements were performed in aerated 3.5% NaCl solution in triply distilled water at the temperature of 25°C, using AUTOLAB 302NFRA32 M [Metrohm-Autolab Instruments Netherlands] workstation, with Nova software. Impedance spectra were recorded at Potential (V) linked with O.C.P. (Open Circuit Potential) value in the frequency range from 0.1 to 60000 Hz, at an amplitude of 5mV. The impedance diagrams are given in the Nyquist plot representation. The IE% was calculated from the charge transfer resistance (R_{ct}) values which were obtained by subtracting the high-frequency impedance using the equation (4). The degree of surface coverage (θ) was calculated using equation (5).

$$IE \ \% = \frac{R_{ct}(in) - R_{ct}(un)}{R_{ct}(in)} \times 100 \ (4)$$

$$\theta = \frac{IE}{100} \ (5)$$

Where; R_{ct} (in) and R_{ct} (un) are the charge transfer resistance of bronze alloy with and without the coating, respectively.
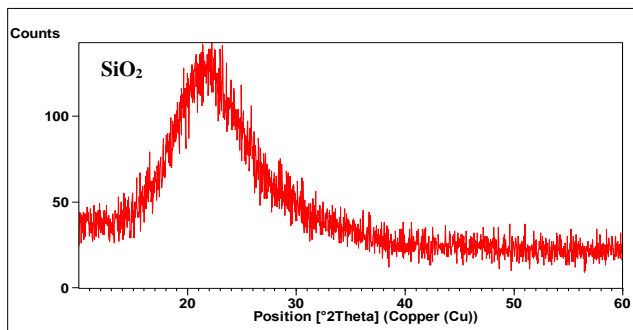
3. Results
3.1. Characterization
The surface morphology examined using TEM revealed the presence of solid monodispersed spherical silica particles, with a well-ordered porous structure. The average particle diameter is approximately 60 ± 5 nm, fig. (1-a & b), while, fig. (1-c) shows the Selected Area Electron Diffraction (SAED) which is a technique used alongside TEM to evaluate the sample's crystallinity, lattice parameters, and crystal structure by evaluating the electron diffraction pattern created by the electron beam's interaction with the sample atoms, it shows the absence of concentric rings confirming that the material

is amorphous. From the XRD pattern, fig. (2), the character-istic diffraction broad peak centered on 23° (2θ) confirmed its amorphous nature.
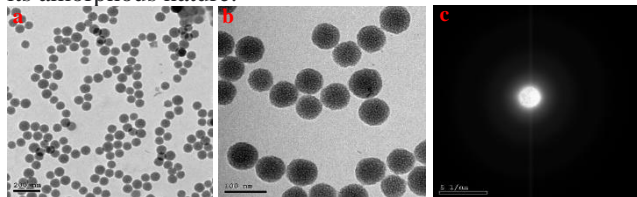
Figure (1) a. & b. TEM image of MP Silica nanoparticles (NPs), **c.** selected area electron diffraction (SAED) confirming that the material is

Figure (2) XRD pattern of the prepared SiO_2 nanoparticles confirming its amorphous nature

The specific surface area, pore volume and pore size distribution measured by nitrogen adsorption– desorption technique provided the results stated in tab (2). Vm is the number of gas molecules that would occupy one cubic centimeter at standard temperature and pressure, as calculated via the ideal gas law is 36.267 cm^3 (STP)g. -1, as BET (specific surface area) is a method to estimate the area per mass of a solid by measuring the gas adsorption on its surface and in its pore. Determining the surface area is important because the functionality of the silica nanoparticles depends on their properties which are often changing as a function of particle size and surrounding medium. General properties are shown in tab (3).

Table (2) the surface area measurements of silica nanoparticles

Vm	36.267	[cm^3(STP) g^-1]
as (BET)	1.58E+02	[m^2 g^-1]
Total pore volume (p/p0=0.9900)	0.5055	[cm^3 g^-1]
Average pore diameter	12.81	[nm]

Table (3) general properties of silica nanoparticles

| Appearance (Color)	White
Appearance (Form)	Powder
Molecular weight	60.08 g/mol
Phase	Amorphous
Size	60±5 nm

3.2. Release study

From the calibration curve, fig. (3), the amount of benzotriazole encapsulated in the mesoporous silica was determined. The curve was created by measuring the absorbance of a series of standard solutions with known concentrations of Benzotriazole ranging from 1 μg mL^{-1} to 50 μg mL^{-1} (3.5% NaCl aqueous solution). The absorbance values were then recorded after the separation of the nanoparticles and plotted against the concentration to create the calibration curve. The concentration of free Benzotriazole was estimated based on the standard curve.

3.2.1. Cal. equation
$$Abs= 0.07244+0.04247*Conc.$$

- I.C= 1000 μg/ml
- Absorbance of free = 0.789
- Concentration of free Benzotriazole (Conc.) = 168.7 μg/ml
- Entrapment efficiency (EE)= 83.13 %

Encapsulation efficiency (EC)= 8.313% w/w is the percentage of inhibitor entrapped into the MSP. The encapsulation efficiency is the amount of benzotriazole that is effectively enclosed with the mesoporous silica nano-containers, while the entrapment efficiency is the amount of Benzotriazole that is released from the nanocontainers once triggered with a suitable stimulus.
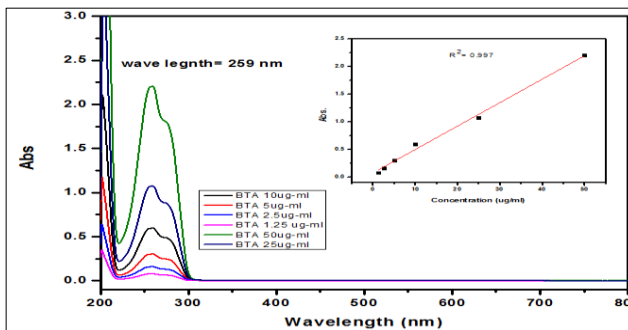
Figure (3) the calibration curve of BTA ranging from a concentration of 1 μg mL−1 to 50 μgml-1 (3.5% NaCl aqueous solution)

The amount of Benzotriazole released at pH levels (5.0, 7.0 and 9.0) was monitored via UV-Vis spectroscopy. The results show the release behavior of the BTA molecules from the mesoporous silica nanocontainers before their dispersion in Paraloid B44 and B72. As shown in fig. (4), the BTA release rate is obvious at different pH values. The presence of two stages of release can be detected which include an induction period (stage I), and sustainable release to level off (stage II). Under acidic conditions, the BTA release is slightly delayed. The accumulative release amount of BTA is at 42% within 100 h at pH 5.0. At neutral conditions, the accumulative release amount of BTA is 61% within 100 h. While in alkaline conditions, the release of BTA accelerated significantly showing 77% at pH 9.0. Clearly the alkaline conditions accelerate the release of BTA compared to the neutral and acidic conditions. These results demonstrate that BTA@MSN is pH sensitive and can be triggered to accelerated release under alkaline condition. However, there is unconstrained leakage of BTA even in neutral conditions.
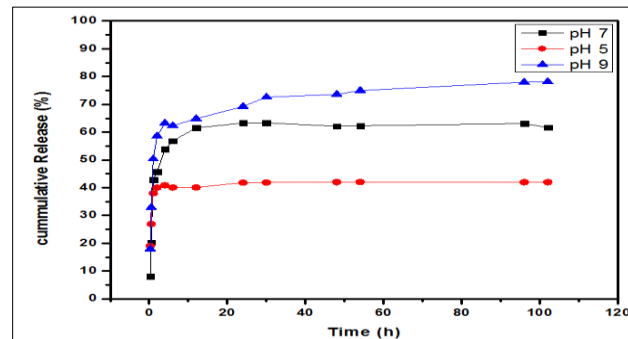

Figure (4) the release kinetics at different pH

3.2.2. Colorimetric measurements

The color change measurement of the coated samples, tab. (4) and fig. (5), revealed that the single coated MSP-B72 samples gave the best results displaying least color change average of ΔE 3.28, while the double coated sample displayed ΔE 3.93, and the single and double coated samples MSP-B44 displayed ΔE 3.54 and ΔE 5.21, respectively. ΔE* values lower than 3 are believed to be not perceivable by the human eye, while those bigger than 5 are. [36] These results demonstrate that the samples coated with MSP/BTA dispersed in Paraloid B-72 show better results than those dispersed in Paraloid B-44. The ΔE of the single layer displayed the least average, and the difference between the single and double layer is minimal.

Table (4) color change measurements (ΔE*) for the coated samples compared to the blank sample

| Samples	Colorimetric Variations				
	L*	A*	B*	EΔ	Image
Blank	65.92	6.37	24.63	-------	-------
MSP – B72 S	63.71	4.67	19.52	3.28	
MSP –B72 D	62.66	3.46	21.45	3.93	
MSP – B44 S	62.24	4.47	22.96	3.54	
MSP –B44 D	63.11	2.85	17.13	5.21	
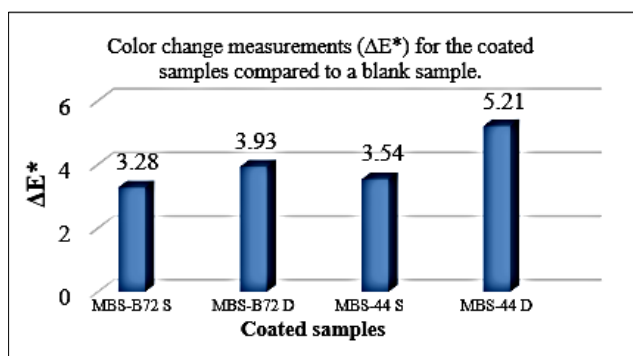
Figure (5) the color change of the coated samples compared to blank

3.3. Electrochemical impedance

EIS technique was applied to study the efficiency of the coating enhanced with mesoporous silica nanocontainers loaded with Benzotriazole, and to evaluate its corrosion protection performance. The results are shown in the form of Nyquist plots in fig. (6-a & b). Using Nova (2.1.2) software, the impedance spectra of the different Nyquist plots were analyzed by fitting the experimental data to a simple equivalent circuit model. Equivalent circuit models help in understanding the development of corrosion and properties of the protective films or coatings. For accurate fitting of experimental impedance data, CPE element was used to represent non-ideal capacitors behavior, which corresponds to the electrode porosity, roughness, inhomogeneity of the surface and non-uniform current distribution [31]. It was found that the equivalent circuit that fit the experimental data consists of model Rs (CPE C

RpW) for the blank bronze coupons and Rs(CPE Rp) for the single and double layer coated bronze alloy electrodes in NaCl solutions as given in tab. (5-a). The circuit representing the blank coupon includes the solution resistance (Rs), constant phase element (CPE), capacitance (C), polarization resistance (Rp) and Warburg impedance. While the circuits representing the single and double layered coated coupons include solution resistance (Rs), constant phase element (CPE), and polarization resistance (Rp). The Impedance parameters for the blank and coated samples are noted in tab. (5-b). The polarization resistance value of the blank coupons is 2.77 Ω, while the values for the samples coated with a single layer of MSP/BTA –B72 is 6.64 Ω with an efficiency of 58.28%. The values for the double layer of MSP/BTA –B72 is 33.5 Ω with an efficiency of 91.73%, which is the highest showing minimal corrosion rate. The values for the single and double MSP/BTA –B44 are 4.27 Ω, with an efficiency of 35.13% and 18.8 Ω with an efficiency of 85.26% respectively. In both coating systems the double layer showed higher efficiency rates.
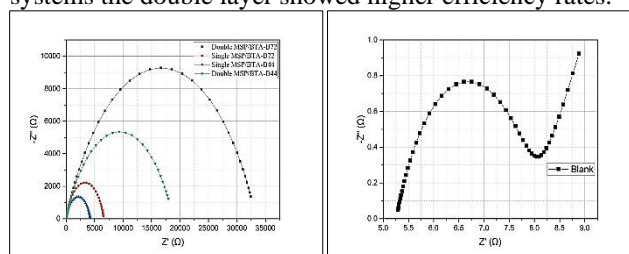

Figure (6) the Nyquist plots of coated samples and blank sample

Table (5-a) the equivalent electrical circuit model used to fit the EIS plots for the single and double coating layers and the blank.

Coating Systems	Rs (Ω cm²)	CPE		Rp (K Ω)	C (μF)	W Y₀(μMho)	IE %	θ
		Y₀(μMho)	n1					
Blank	5.26	4.77	0.637	2.77	110	993	------	------
Single MSP/BTA –B72	6.05	6.01	0.751	6.64	------	------	58.28	0.5828
Double MSP/BTA –B72	-57.3	2.06	0.645	33.5	------	------	91.73	0.9173
Single MSP/BTA –B44	-4.97	2.44	0.715	4.27	------	------	35.13	0.3513
Double MSP/BTA –B44	-10.5	5.98	0.658	18.8	------	------	85.26	0.8526

Table (5-b) impedance parameters for the blank and coated samples in 3.5% NaCl solution operated at room temperature
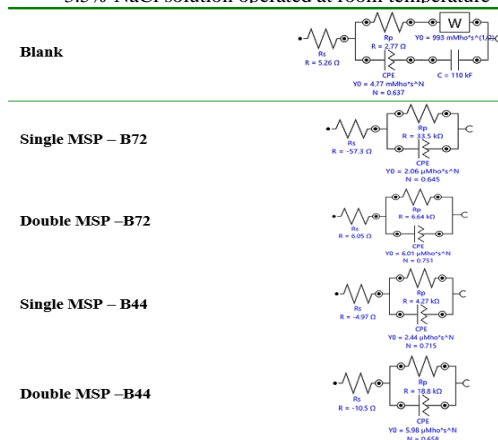
4. Discussion

Smart self-healing coatings present significant advancements in protecting metallic artifacts by offering innovative solutions to prevent corrosion and damage. These coatings can independently repair minor defects, reducing the need for frequent

maintenance, conserving resources, and extending the lifespan of artifacts. Additional benefits include controlled delivery of active ingredients, making encapsulation particularly valuable in corrosion protection. The combined potential of these features promotes more sustainable and efficient preservation practices in cultural heritage conservation [38,39]. In encapsulation systems, coatings usually consist of a polymer matrix and a nano capsule, which generally has two key components: the shell and the core. The shell serves as a protective barrier, requiring high thermal stability and appropriate mechanical properties, while the core contains the corrosion inhibitor, which heals damaged areas. This action is triggered by an external corrosion related stimuli [40,41]. However, these advanced coatings have some limitations such as finite nature of the self-healing function—once the active species are depleted, the coating loses its ability to repair itself [42]. Mesoporous silica nanoparticles (MSNs) were selected in this study because of their high specific surface area, thermal and mechanical stability, availability, low cost, and suitability for use in different coating layers. Following the synthesis and characterization of the MSNs, Benzotriazole (BTA) a heterocyclic compound with the chemical formula $C_6H_5N_3$, an effective corrosion inhibitor for copper and its alloys was encapsulated within the nanocontainers. The encapsulated BTA were dispersed into 3% Paraloid B72 and B44 in acetone by sonication and applied into cast bronze coupons with composition similar to archaeological bronze artefacts. The encapsulation and entrapment efficiency of BTA was determined. The amount of Benzotriazole released at pH levels (5.0, 7.0 and 9.0) was monitored via UV-Vis spectroscopy. The results indicate that alkaline conditions accelerate the release of BTA compared to neutral and acidic conditions, confirming that BTA@MSN is pH-sensitive and can be triggered for accelerated release under alkaline conditions. These results are comparable to those obtained by Wen [31], where the pH-sensitive release property of BTA@MSNs-COOH-PEI was assessed using UV-Vis spectroscopy, showing that the release rate of benzotriazole (BTA) increases under alkaline conditions. However, it was observed that BTA leakage persisted even under neutral conditions, which suggests a need for further investigation. Calorimetry confirmed the possibility of the use of a single coat of BTA@MSN dispersed in Paraloid B-72 with minimal impact on the aesthetic attributes and surface appearance. The corrosion inhibitive performance of the coating was also verified, with the highest performance observed in the case of applying a double coat of BTA@MSN dispersed in Paraloid B-72.

5. Conclusion

The performance of the BTA-Loaded Mesoporous silica nanocontainers added to Paraloid B-44 and B72 was investigated using various techniques, such as release study, colorimetric measurements and electrochemical impedance spectroscopy (EIS). The sustained release of Benzotriazole to varying pH levels was confirmed. The release was higher with an increase in the pH of the medium, which signify that the release rate is more in alkaline medium compared to the neutral and acidic. These results demonstrate that BTA@MSN is pH sensitive and can be triggered to accelerated release under alkaline condition. Further studies will be performed for the study of

delayed release under acidic conditions The colorimetric measurements revealed that the samples coated with a single layer MSP/BTA dispersed in Paraloid B-72 showed the best results compared to those dispersed in Paraloid B-44. And whilst the ΔE of the single layer displayed the least average, but the difference between the single and double layer is minimal. The electrochemical impedance spectroscopy values for the double layer of MSP/BTA –B72 is 33.5 Ω with an efficiency of 91.73%, which is the highest showing minimal corrosion rate. The use of BTA-Loaded Mesoporous silica nanocontainers added to polymer coatings showed promising results for the corrosion protection of archaeological bronze artefacts in museum environments by preventing the uncontrolled leaching of inhibitor from the coating material and to circumvent direct interaction between the coating polymer and inhibitor. This approach facilitates controlled release of the active inhibitor from the coating material.

References

[1] Andreeva, D., Fix, D., Möhwald, H., et al. (2008). Self-healing anticorrosion coatings based on pH-sensitive polyelectrolyte/inhibitor sandwich like nanostructures. *Adv. Mater*. 20: 2789-2794.

[2] Ferreira, M., Zheludkevich, M., Tedim, J., et al. (2012). Self-healing nanocoatings for corrosion control. In: Saji, S. & Cook, R. (Eds.) *Metals and Surface Engineering, Corrosion Protection and Control Using Nanomaterials*, Woodhead Publishing, UK, pp. 213-263.

[3] Rani B. & Basu, B. (2012). Green inhibitors for corrosion protection of metals and alloys: An overview, *Int. J. of Corrosion*. 2012: 1687-9325

[4] Ávila-Gonzalez, A., Cruz-Silva, R., Menchaca, C., et al. (2011). Use of silica tubes as nanocontainers for corrosion inhibitor storage. *J. of Nanotechnology*. 11 (1), doi:10.1155/2011/461313.

[5] Stankiewicz, A. Szczygieł, I. & Szczygieł, B. (2013). Self-healing coatings in anti-corrosion applications. *J. Mater Sci*. 48: 8041-8051.

[6] Garcia-Heras, M., Jimenez-Morales, A., Casal, B., et al. (2004). Preparation and electrochemical study of cerium-silica sol-gel thin films. *J. Alloys Compd*. 380: 219-224.

[7] Montemor, M. (2014). Functional and smart coatings for corrosion protection: A review of recent advances. *Surface & Coatings Technology*. 258 :17-37.

[8] Vreugdenhil, A. & Woods, M. (2005). Triggered release of molecular additives from epoxy-amine sol-gel coatings. *Prog. Org. Coatings*. 53: 119-125.

[9] Shchukin, D. & Möhwald, H. (2007). Self-repairing coatings containing active nanoreservoirs, *Small*. 3 (6): 926-943.

[10] Raps, D., Hack, T., Wehr, J., et al. (2009). Electrochemical study of inhibitor-containing organic-inorganic hybrid coatings on AA 2024. *Corrosion Science*. 51 (5): 1012-1021.

[11] Kartsonakis, I., Balaskas, A., Koumoulos, E., et al. (2012). Evaluation of corrosion resistance of magnesium alloy ZK10 coated with hybrid organic–inorganic film including containers. *Corrosion Science*. 65: 481-493.

[12] Xu, H., Zhang, H., Wang, D., et al. (2015). A facile route for rapid synthesis of hollow mesoporous silica nanoparticles as pH-responsive delivery carrier. *J. Colloid Interf Sci*. 451: 101-107.

[13] Shchukin, D., Zheludkevich, M., Yasakau, K., et al. (2006). Layer-by-layer assembled nanocontainers for self-healing corrosion protection. *Materials Science, Engineering Chemistry*. 16: 4561-4566.

[14] Matsuda, T., Jadhav, N., Kashi, K., et al. (2019). Release behavior of pH sensitive microcapsules containing corrosion inhibitor. *Progress in Organic Coatings*. 132: 9-14.

[15] Zea, C., Barranco-García, R., Alcántara, J., et al. (2018). pH-dependent release of environmentally friendly corrosion inhibitor from mesoporous silica nanoreservoirs, *Microporous & Mesoporous Materials*. 255: 166-173.

[16] Roberge, P. (2008). *Corrosion engineering: Principles and Practice*, McGraw-Hill, USA.

[17] Borisova, D., Möhwald, H. & Shchukin, D. (2013). Influence of embedded nanocontainers on the efficiency of active anticorrosive coatings for aluminum alloys part II: Influence of nanocontainer position. *ACS Appl Mater & Interfaces*. 5 (1): 80-87.

[18] Saremi, M. & Yeganeh, M. (2014). Application of mesoporous silica nanocontainers as smart host of corrosion inhibitor in polypyrrole coatings. *Corrosion Science*. 86: 159-170.

[19] Liu, X., Zhang, H., Wang, J., et al. (2012). Preparation of epoxy microcapsule based self-healing coatings and their behavior. *Surf. Coat. Technol*. 206: 4976-4980.

[20] Qiao, Y., Li, W., Wang, G., et al. (2015). Application of ordered mesoporous silica nanocontainers in an anticorrosive epoxy coating on a magnesium alloy surface. *RSC Adv*. 5: 47778-47787.

[21] Stöber, W., Fink, A. & Bohn, E., (1968). Controlled growth of monodisperse silica spheres in the micron size range. *J. Colloid Interface Sci*. 26 (1): 62-69.

[22] Ha, C. & Park, S. (2018). General synthesis and physicochemical properties of mesoporous materials. In: SSMATERIALS (ed.) *Periodic Mesoporous Organosilicas*. 281: 15-85.

[23] Vijayan P. & Al-Maadeed, M. (2016). TiO$_2$ nanotubes and mesoporous silica as containers in self-healing epoxy coatings. *Scientific Reports*. 6, doi: 10.1038/ srep38812.

[24] Song, N. & Yang, Y. (2015). Molecular and supramolecular switches on mesoporous silica nanoparticles. *Chem. Soc. Rev*. 44: 3474-3504.

[25] Hassan, A. (2015). Biocompatible SiO$_2$ in the fabrication of stimuli-responsive hybrid composites and their application potential. *J. Chemistry*. 2015, doi:10. 1155/2015/846328.

[26] Yamada, Y. & Yano, K. (2006). Synthesis of monodispersed super-microporous/mesoporous silica spheres with diameters in the low submicron range. *Microporous Mesoporous Mater*. 93 (1-3): 190-198.

[27] Radu, D., Lai, C., Huang, J., et al. (2005). Fine-tuning the degree of organic functionalization of mesoporous silica nanosphere materials via an interfacially designed co-condensation method. *Chem. Commun*. 10: 1264-1266.

[28] Olivieri, F., Castaldo, R., Cocca, M., et al. (2021). Mesoporous silica nanoparticles as carriers of active agents for smart anticorrosive organic coatings: A critical review. *Nanoscale*. 13: 9091-9111.

[29] Chen, Y., Chen, H., Guo, L., et al. (2010). Hollow/rattle-type mesoporous nanostructures by a structural difference-based selective etching strategy. *ACS Nano*. 4 (1): 529-539.

[30] Sanyal, S., Park, S., Chelliah, R., et al. (2024). Emerging trends in smart self-healing coatings: A focus on micro/nanocontainer technologies for enhanced corrosion protection. *Coatings*. 14 (3), doi: 10.3390/coatings1403-0324

[31] Wen, J., Lei, J., Chen, J., et al. (2020). Polyethylenimine wrapped mesoporous silica loaded benzot-iazole with high pH-sensitivity for assembling self-healing anti-corrosive coatings. *Materials Chemistry and Physics*. 253 doi: 10.1016/j.matchemphys.2020.123425.

[32] Karekar, S., Bagale, U., Sonawane, Sh., et al. (2018). Composite interfaces, a smart coating established with encapsulation of zinc molybdate centred nanocontainer for active corrosion protection of mild steel: release kinetics of corrosion inhibitor. *Composite Interfaces*, doi: 10.1080/09276440.2018.1439631.

[33] De-Luna, M., Buonocore, G., Di Carlo, G., et al. (2016). Protection of bronze artefacts through polymeric coatings based on nanocarriers filled with corrosion inhibitors. In: D'Amore, A., Acierno, D. & Grassia, L. (eds.) *VIII Int. Conf. on "Times of Polymers and Composites": From Aerospace to Nanotechnology*, AIP Publishing, USA, 1736 (1), doi: 10.1063/1.4949623.

[34] Wanyika, H., Gatebe, E. & Kioni, P., (2011) Synthesis and characterization of ordered mesoporous silica nanoparticles with tunable physical properties by varying molar composition of reagents. *African J. of Pharmacy and Pharmacology*. 5 (21): 2402-2410.

[35] ASTM (1995). *Annual book of ASTM standards, D-1 on paints, related coatings, materials, and applications and are the direct responsibility of subcommittee D01.23 on physical properties of applied paint film, D1640-95: Standard test methods for drying, curing, or film formation of organic coatings at room temperature,* American Society for Testing and Materials, USA.

[36] Islami, M., Zarrabi, A., Tada, S., et al. (2018). Controlled quercetin release from high-capacity-loading hyperbranched polyglycerol-functionalized graphene oxide. *Int J Nanomedicine*. 13: 6059-6071,

[37] Albini, M. (2017). *Fungal biogenic patina: Optimization of an innovative conservation treatment for copper-*

based artefacts, Ph.D, Lab. of Technologies for Heritage Materials and Lab. of Microbiology, Faculty of Science, University of Neuchâtel, Switzerland.

[38] Sonawane, S., Bhanvase, B., Jamali, A., et al. (2012). Improved active anticorrosion coatings using layer-by-layer assembled ZnO nanocontainers with benzotriazole. *Chemical Engineering J*. 189-190: 464-472.

[39] Li, W., Buhrow, J. & Jolley, S. (2015). Microencapsulation technologies for corrosion protective coating applications. *J. of Coatings Technology and Research*. 12 (4): 643-659.

[40] Kothari, J. & Iroh, J. (2023). Self-healing poly(urea formaldehyde) Microcapsules: Synthesis and Characterization. *Polymers*. 15 (7), doi: 10.3390/polym15071668.

[41] Kontiza, A. & Kartsonakis, I. A. (2024). Smart composite materials with self-healing properties: A review on design and applications. *Polymers*. 16 (15), doi: 10.3390/polym16152115

[42] Zhang, R., Yu, X., Yang, Q., et al. (2021). The role of graphene in anti-corrosion coatings: A review. *Construction and Building Materials*. 294 (2), doi: 10.1016/j.conbuildmat.2021.123613.